Exact Coherent States: Theory & Methods

Rich Kerswell

Lectures 1 & 2

DRAFT May 20, 2019

1 Finite Amplitude Solutions

In the previous lecture by Marc Avila, we heard about linear instabilities. Each of these leads to a new type of exact solution to the governing equations. To demonstrate this, we now study what happens to this linear instability as it grows in amplitude. To underpin our understanding we first consider a *weakly nonlinear analysis* of the bifurcation which assumes small amplitudes before discussing branch continuation to larger amplitudes. To give the discussion some context we consider rotating plane Couette flow (a straightened out version of Taylor-Couette flow): see figure 1. The governing Navier-Stokes equations for an incompressible flow are

$$\frac{\partial \mathbf{u}_{\text{tot}}}{\partial t} + 2\Omega\hat{\mathbf{z}} \times \mathbf{u}_{\text{tot}} + \mathbf{u}_{\text{tot}} \cdot \nabla\mathbf{u}_{\text{tot}} + \nabla p = \frac{1}{Re}\nabla^2\mathbf{u}_{\text{tot}}, \tag{1}$$

$$\nabla \cdot \mathbf{u}_{\text{tot}} = 0, \tag{2}$$

and the boundary conditions for rotating plane Coeutte flow are $\mathbf{u}_{\text{tot}}(x, \pm 1, z, t) = \pm\hat{\mathbf{x}}$ where $\mathbf{\Omega} = \Omega\hat{\mathbf{z}}$ is the spanwise rotation rate. We define $\mathbf{u}_{\text{tot}} = \mathbf{u}_{\text{lam}} + \hat{\mathbf{u}}$, where $\hat{\mathbf{u}} := (\hat{u}, \hat{v}, \hat{w})$ is a (possibly large) perturbation to the laminar base state $\mathbf{u}_{\text{lam}} := y\hat{\mathbf{x}}$ so that the full perturbation equations are

$$\frac{\partial \hat{\mathbf{u}}}{\partial t} + 2\Omega\hat{\mathbf{z}} \times \hat{\mathbf{u}} + \mathbf{u}_{\text{lam}} \cdot \nabla\hat{\mathbf{u}} + \hat{\mathbf{u}} \cdot \nabla\mathbf{u}_{\text{lam}} + \hat{\mathbf{u}} \cdot \nabla\hat{\mathbf{u}} + \nabla\hat{p} = \frac{1}{Re}\nabla^2\hat{\mathbf{u}}, \tag{3}$$

$$\nabla \cdot \hat{\mathbf{u}} = 0, \tag{4}$$

where now $\hat{\mathbf{u}}(x, \pm 1, z, t) = \mathbf{0}$.

1.1 Linear stability

Linearising equation (3) gives

$$\frac{\partial \hat{\mathbf{u}}}{\partial t} + 2\Omega\hat{\mathbf{z}} \times \hat{\mathbf{u}} + \mathbf{u}_{\text{lam}} \cdot \nabla\hat{\mathbf{u}} + \hat{\mathbf{u}} \cdot \nabla\mathbf{u}_{\text{lam}} + \nabla\hat{p} = \frac{1}{Re}\nabla^2\hat{\mathbf{u}}. \tag{5}$$
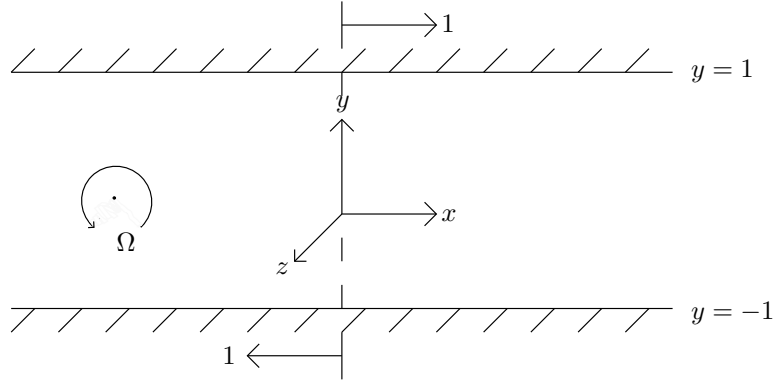
Figure 1: (Spanwise) Rotating Plane Couette flow

Assuming streamwise Taylor (2D) roll solutions of the form

$$\hat{\mathbf{u}}(\mathbf{x}, t) = \tilde{\mathbf{u}}(y)e^{ikz+\sigma t} \tag{6}$$

(5) becomes

$$\sigma\tilde{\mathbf{u}} + \begin{bmatrix} (1-2\Omega)\tilde{v} \\ 2\Omega\tilde{u} \\ 0 \end{bmatrix} + \nabla\tilde{p} = \frac{1}{Re}\nabla^2\tilde{\mathbf{u}}. \tag{7}$$

Eliminating $\hat{w}$ using the incompressibility condition, $\hat{p}$ from $\hat{\mathbf{z}}.(7)$ and $\hat{u}$ from $\hat{\mathbf{x}}.(7)$ leaves

$$2Re^2\Omega(1-2\Omega)k^2\tilde{v} = -(D^2 - k^2 - \sigma Re)^2(D^2 - k^2)\tilde{v}, \tag{8}$$

to be solved subject to boundary conditions

$$\tilde{v} = D\tilde{v} = (D^2 - k^2 - \sigma Re)(D^2 - k^2)\tilde{v} = 0 \text{ at } y = \pm 1, \tag{9}$$

where $D := \mathrm{d}/\mathrm{d}y$. The objective is to find $Re_L = \min_k Re$ such that $\Re e(\sigma) = 0$. Conveniently, this can be done by comparing it to the (famous and classical) Rayleigh-Bénard convection problem given by

$$k^2 Ra\,\tilde{w} = -(D^2 - k^2 - \sigma)^2(D^2 - k^2)\tilde{w} \tag{10}$$

with boundary conditions

$$\tilde{w} = D\tilde{w} = (D^2 - k^2 - \sigma)(D^2 - k^2)\tilde{w} = 0 \text{ at } y = \pm\frac{1}{2}, \tag{11}$$

where Ra is the Rayleigh number. This system has a well-known solution,

$$\min_k Ra = 1708 \quad \text{for} \quad \sigma = 0 \ \& \ k = 3.117 \tag{12}$$

(Drazin 2002, §6.3 and the rigid-rigid case). Since the layer depth for Rayleigh-Bénard convection is standardly non-dimensionalised to be 1 whereas it is 2 here (e.g.

2

compare positions of boundaries), the lengths in equations (8) and (9) need to be rescaled to make the connection exact. Letting $D^2 \to \frac{1}{4}D^2$, $k^2 \to \frac{1}{4}k^2$ and setting $\sigma = 0$ in (10) means the association

$$Re_L^2 = \frac{1708}{2^4[2\Omega(1 - 2\Omega)]} \tag{13}$$

can be made. The minimum of Re_L occurs when $\Omega = 1/4$ and is

$$\min_{k,\Omega} Re_L = 20.67. \tag{14}$$

Notice that $Re_L \to \infty$ for $\Omega \to 0$ and $1/2$. Beyond these values, there is no linear instability: the Rayleigh number in the analogous Rayleigh-Benard problem is then negative indicating that the stationary fluid is hotter on its top surface than the bottom which is a very stable situation.

1.2 Weakly Nonlinear Analysis

Now we consider what happens to this linear instability for Re slightly away from the bifurcation point. For convenience we rewrite (3) as

$$\mathcal{L}(\Omega, Re)\hat{\mathbf{u}} = -\hat{\mathbf{u}} \cdot \nabla\hat{\mathbf{u}} \tag{15}$$

and consider an expansion around the critical point $(\Omega^*, Re_L(\Omega^*))$ as defined in (13). For simplicity, we take $\Omega^* = 1/4$ (so $Re_L = 20.67$) and only consider a small change in Re. Specifically let $Re = Re_L + \varepsilon^2 Re_1$ so that ε is *defined* as $\sqrt{(Re - Re_L)/Re_1} \ll 1$ where Re_1 is unknown and may be positive (negative) indicating the branch bends towards increasing (decreasing) Re. and let

$$\hat{\mathbf{u}}(\mathbf{x}) := \varepsilon[\mathbf{u}_1(y)e^{ikz} + \mathbf{u}_{-1}e^{-ikz}] + \varepsilon^2[\mathbf{u}_0(y) + (\mathbf{u}_2(y)e^{2ikz} + \mathbf{u}_{-2}(y)e^{-2ikz})]$$
$$+\varepsilon^3[\mathbf{v}_1(y)e^{ikz} + \mathbf{v}_{-1}e^{-ikz}) + (\mathbf{v}_3(y)e^{3ikz} + \mathbf{v}_{-3}(y)e^{-3ikz})] + \mathcal{O}(\varepsilon^4) \tag{16}$$

where since $\hat{\mathbf{u}}$ is real, $\mathbf{u}_{-m}(y) = \mathbf{u}_m^*(y)$ and there is an accompanying expansion for p. Since the bifurcation is steady (a pitchfork), no time dependence is included and ε measures the amplitude of the solution branch as $\varepsilon \to 0$. Let also

$$\mathcal{L}(Re_L + \varepsilon^2 Re_1) = \mathcal{L}_0(Re_L) + \varepsilon^2 Re_1 \mathcal{L}_1 + \dots. \tag{17}$$

Then there is a hierarchy of problems as follows

$$\mathcal{O}(\varepsilon): \qquad \mathcal{L}_0\mathbf{u}_1(y)e^{ikz} = 0 \quad \text{(the linear problem)} \tag{18a}$$

$$\mathcal{O}(\varepsilon^2): \qquad \mathcal{L}_0\mathbf{u}_0(y) = -\mathbf{u}_1e^{ikz} \cdot \nabla\mathbf{u}_{-1}e^{-ikz} - \mathbf{u}_{-1}e^{-ikz} \cdot \nabla\mathbf{u}_1e^{ikz} \tag{18b}$$

$$\mathcal{L}_0\mathbf{u}_2(y)e^{2ikz} = -\mathbf{u}_1e^{ikz} \cdot \nabla\mathbf{u}_1e^{ikz} \tag{18c}$$

$$\mathcal{O}(\varepsilon^3): \qquad \mathcal{L}_0\mathbf{v}_1(y)e^{ikz} = -\mathbf{u}_1e^{ikz} \cdot \nabla\mathbf{u}_0 - \mathbf{u}_0 \cdot \nabla\mathbf{u}_1e^{ikz} - \mathbf{u}_{-1}e^{-ikz} \cdot \nabla\mathbf{u}_2e^{2ikz}$$
$$- \mathbf{u}_2e^{2ikz} \cdot \nabla\mathbf{u}_{-1}e^{-ikz} - Re_1\mathcal{L}_1\mathbf{u}_1e^{ikz}. \tag{18d}$$

$$\mathcal{L}_0\mathbf{v}_3(y)e^{3ikz} = \dots.$$

on substituting into the Navier-Stokes equations. The key point here is that $\mathcal{L}_0$ has a non-trivial kernel - see (18a) - so (18d) only has a solution if the following solvability condition is satisfied

$$\langle \mathbf{u}_0^+ e^{ikz}, \mathcal{L}_0 \mathbf{v}_1 e^{ikz} \rangle = -\left\langle \mathbf{u}_1 e^{ikz} \cdot \nabla \mathbf{u}_0 + \mathbf{u}_0 \cdot \nabla \mathbf{u}_1 e^{ikz} + \mathbf{u}_{-1} e^{-ikz} \cdot \nabla \mathbf{u}_2 e^{2ikz} \right. \tag{19}$$
$$\left. + \mathbf{u}_2 e^{2ikz} \cdot \nabla \mathbf{u}_{-1} e^{-ikz} \right\rangle - Re_1 \langle \mathbf{u}_0^+, \mathcal{L}_1 \mathbf{u}_1 e^{ikz} \rangle$$

where $\mathcal{L}_0^+[\mathbf{u}_0^+(y)e^{ikz}] = 0$ ($\mathbf{u}_0^+(y)e^{ikx}$ spans the kernel of $\mathcal{L}_0^+$, the adjoint of $\mathcal{L}_0$ under the inner product $\langle A, B \rangle := \int A^* B \, dV$). Since the *lhs* vanishes,

$$\langle \mathbf{u}_0^+ e^{ikz}, \mathcal{L}_0 \mathbf{v}_1 e^{ikz} \rangle = \langle \mathcal{L}_0^+ \mathbf{u}_0^+ e^{ikz}, \mathbf{v}_1 \rangle = 0, \tag{20}$$

the vanishing of the *rhs* is a real condition which defines Re_1 (as opposed to a generally complex condition which would also specify the frequency change if there was one) and there is then a precise relationship between the change in Re from the bifurcation point and the amplitude of the bifurcated solution. This analysis shows nicely how: 1) the marginal eigenfunction is the foundation of the expansion and that 2) higher and higher harmonics of the maginal eigenfunction are systematically generated by the advective nonlinearity as the amplitude grows. If we are a finite distance away from the bifurcation point, we need a fully numerical approach.

1.3 Branch Continuation

A solution branch can be traced out by considering the complete 2D velocity expansion

$$\begin{bmatrix} \mathbf{u}(y, z) \\ p(y, z) \end{bmatrix} = \sum_{\ell=-\infty}^{+\infty} \begin{bmatrix} \tilde{\mathbf{u}}_\ell(y) \\ \tilde{p}_\ell(y) \end{bmatrix} e^{i\ell kz} \tag{21}$$

truncated to some finite positive upper and negative lower values (say, $\pm L$) in ℓ where k is the critical wavenumber (the weakly nonlinear expansion of (1.2) would just have $\ell = 0, \pm1, \pm2$ only). The expansion functions $\tilde{\mathbf{u}}_\ell(y)$ and $\tilde{p}_\ell$ are typically themselves expanded in terms of global basis functions in y so that the solution is represented by a doubly-indexed set of complex coefficients (finite differencing in y is also an alternative). For example, Chebyshev polynomials $T_n(y)$ are a popular choice because they are easily defined,

$$T_n(y) := \cos(n \cos^{-1} y) \qquad \text{(so } T_0 = 1; \ T_1 = y; \ T_2 = 2y^2 - 1; \ T_3 = 4y^3 - 3y \text{ etc)}, \tag{22}$$

(see figure 2) and are very efficient at representing functions which are specified at boundaries (e.g. [9]). If N is the largest order Chebyshev polynomial retained, there are $N + 1$ coefficients for every velocity component and the pressure for each Fourier wavenumber, or, in other words $NT := 4(N + 1)(L + 1)$ complex degrees
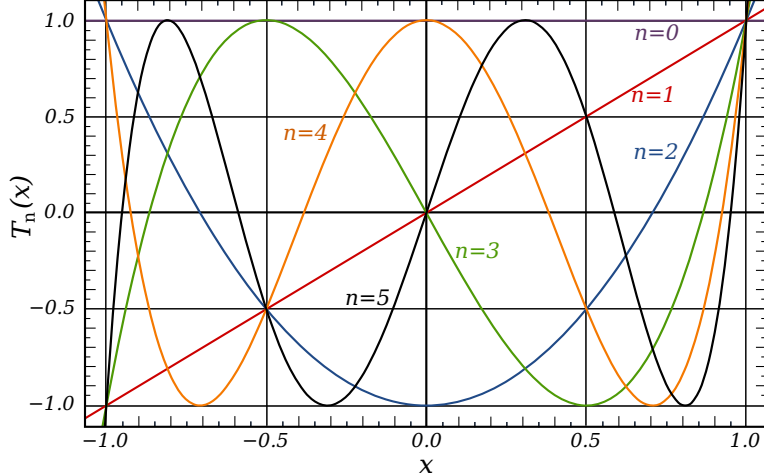
4

Figure 2: Chebyshev polynomials

of freedom (the fact that the physical fields are real means we don't need to store negative wavenumbers giving the factor $(L+1)$ rather than $(2L+1)$). We need the same number of independent equations to compute a solution. These are obtained by substituting (21) into the Navier-Stokes equations and then splitting the results (most simply rearranged into the three components of the Navier-Stokes equations and the incompressibility condition) into components corresponding to a specific wavenumber. The result can be further split to reflect the Chebyshev expansion. There are two main methods: Galerkin projection using the fact that

$$\int_{-1}^{1} \frac{T_n(y)T_m(y)}{\sqrt{1-y^2}}dy = \begin{cases} 0 & n \neq m \\ \pi & n = m = 0 \\ \pi/2 & n = m \neq 0 \end{cases} \tag{23}$$

to decompose the equations into their respective Chebyshev expansion or collocation where the equations are evaluated at (N+1) sample points y_j across the domain (the $N+1$ zeros of $T_{N+1}(y)$ is a convenient choice which ensures exponential convergence). Boundary conditions are imposed by replacing some of the equations typically near to the appropriate boundary or corresponding to the highest order Chebyshev components.

The above procedure gives $4(N+1)(L+1)$ quadratically-nonlinear algebraic equations for all coefficients of the double expansions. Solutions are then found using root-finding algorithms invariably based upon the Newton-Raphson method. To find a solution of $\mathbf{F}(\mathbf{u}; Re) = \mathbf{0}$ where $\mathbf{F}$ and $\mathbf{u} \in \mathbb{C}^{NT}$, Newton Raphson proceeds by taking a guess $\mathbf{u}_n$ and generating another $\mathbf{u}_{n+1}$ via

$$\mathbf{u}_{n+1} = \mathbf{u}_n - \mathbf{J}^{-1}\mathbf{F}(\mathbf{u}_n, Re) \tag{24}$$

where $J_{ij} := \partial F_i/\partial u_j$ is the Jacobian and is an $NT \times NT$ sized complex matrix. How large can NT be before things become impractical using direct matrix solvers? Just

20 years ago, NT would be limited to O(5,000) (or O(10,000) for a real matrix) on a 32-bit machine with a maximum memory of 2GB. Now O(100,000) is possible on a 512GB machine and runtimes are made acceptable by multithreaded linear algebra routines (e.g. BLAS libraries). Bigger jobs need a different approach - see Marc Avila's lecture on iterative Krylov methods and [10] for a brief history. This has lead in the past to calculations being focussed on more symmetric solutions - its worth appreciating why.

1.4 Symmetries

Consider the Navier-Stokes equations for pipe flow written for the disturbance away from the base state, $\mathbf{u} := \mathbf{u}_{tot} - (1 - s^2)\hat{\mathbf{z}}$,

$$\frac{\partial \mathbf{u}}{\partial t} = \mathbf{f}(\mathbf{u}) := -(1 - s^2)\frac{\partial \mathbf{u}}{\partial z} + 2su\hat{\mathbf{z}} - \mathbf{u} \cdot \nabla \mathbf{u} - \nabla p + \frac{1}{Re}\nabla^2 \mathbf{u} \tag{25}$$

with $\nabla \cdot \mathbf{u} = 0$ and boundary conditions $\mathbf{u}(1, \phi, z) = \mathbf{0}$ and $(\mathbf{u}, p)(s, \phi, z + 2\pi/\alpha) = (\mathbf{u}, p)(s, \phi, z)$ i.e. the flow is periodic in z with a wavenumber α. We now show that:

(a) these equations and boundary conditions have the Shift-&-Reflect symmetry,

$$\mathcal{S} : (u, v, w, p)(s, \phi, z) \rightarrow (u, -v, w, p)(s, -\phi, z + \pi/\alpha); \tag{26}$$

(b) that since u_{lam} is symmetric under $\mathcal{S}$ - i.e. $\mathcal{S}\mathbf{u}(\mathbf{x}) = \mathbf{u}(\mathcal{S}\mathbf{x})$ - the linear stability problem can be partitioned into considering only $\mathcal{S}$-symmetric and $\mathcal{S}$-antisymmetric disturbances separately; and

(c) branch continuing a $\mathcal{S}$-symmetric instability will lead to a nonlinear solution in a $\mathcal{S}$-symmetric subspace whereas branch continuing a $\mathcal{S}$-antisymmetric instability will *not* be contained within a $\mathcal{S}$-antisymmetric subspace.

Firstly, we need to show that

$$\mathcal{S}\frac{\partial \mathbf{u}}{\partial t} = \mathcal{S}\mathbf{f}(\mathbf{u}) = \mathbf{f}(\mathcal{S}\mathbf{u}). \tag{27}$$

Just consider 3rd component (for brevity), inserting $\mathcal{S}\mathbf{u}$ into $\hat{\mathbf{z}}.\mathbf{f}$ gives

$$\begin{aligned}
\hat{\mathbf{z}} \cdot \mathbf{f}(\mathcal{S}\mathbf{u}) &= -(1 - s^2)\frac{\partial w}{\partial z} + 2su - u\frac{\partial w}{\partial s} - \frac{(-v)}{s}\left(-\frac{\partial w}{\partial \phi}\right) - w\frac{\partial w}{\partial z} - \frac{\partial p}{\partial z} \\
&\quad - \frac{1}{Re}\left[\frac{1}{s}\frac{\partial}{\partial s}\left(s\frac{\partial w}{\partial s}\right) + \frac{1}{s^2}\left(-\frac{\partial}{\partial \phi}\right)\left(-\frac{\partial w}{\partial \phi}\right) + \frac{\partial^2 w}{\partial z^2}\right] \\
&= -(1 - s^2)\frac{\partial w}{\partial z} + 2su - u\frac{\partial w}{\partial s} - \frac{v}{s}\frac{\partial w}{\partial \phi} - w\frac{\partial w}{\partial z} - \frac{\partial p}{\partial z} \\
&\quad - \frac{1}{Re}\left[\frac{1}{s}\frac{\partial}{\partial s}\left(s\frac{\partial w}{\partial s}\right) + \frac{1}{s^2}\frac{\partial^2 w}{\partial \phi^2} + \frac{\partial^2 w}{\partial z^2}\right] \\
&= \hat{\mathbf{z}} \cdot \mathcal{S}\mathbf{f}(\mathbf{u}) \tag{28}
\end{aligned}$$

as required. The other components (including incompressibility) and the b.c.s behave similarly so the system is $\mathcal{S}$-*equivariant*. This *doesn't* mean the solutions have to be $\mathcal{S}$-symmetric but it does mean that if there is a solution $\mathbf{u}$, then $\mathcal{S}\mathbf{u}$ is also a solution. Hence uniqueness implies the solution is $\mathcal{S}$-symmetric.

Moving on to (b) linearizing the system (i.e make the small amplitude assumption of $\mathbf{u}$ around $\mathbf{u}_{lam}$) and assuming $\mathbf{u}(\mathbf{x}, t) = \mathbf{u}(\mathbf{x})e^{\sigma t}$ is an eigenfunction, then

$$\sigma\mathbf{u} = \mathbf{Lu} \qquad \text{where} \quad \mathbf{Lu} := -(1-s^2)\frac{\partial\mathbf{u}}{\partial z} + 2su\hat{\mathbf{z}} - \nabla p + \frac{1}{Re}\nabla^2\mathbf{u}. \qquad (29)$$

Since $\mathbf{f}$ and $\mathbf{u}\cdot\nabla\mathbf{u}$ are $\mathcal{S}$-equivariant, so is $\mathbf{L} = \mathbf{f} + \mathbf{u}\cdot\nabla\mathbf{u}$ and since it is linear in $\mathbf{u}$

$$\sigma(\mathcal{S}\mathbf{u}) = L(\mathcal{S}\mathbf{u}) \quad \Rightarrow \quad \sigma(\mathbf{u}\pm\mathcal{S}\mathbf{u}) = \mathbf{L}(\mathbf{u}\pm\mathcal{S}\mathbf{u}) \qquad (30)$$

where, for *any* initial eigenfunction $\mathbf{u}$, $\mathbf{u}_S := \mathbf{u} + \mathcal{S}\mathbf{u}$ is a $\mathcal{S}$-symmetric version (i.e. $\mathcal{S}\mathbf{u}_S = \mathbf{u}_S$) and $\mathbf{u}_A := \mathbf{u} - \mathcal{S}\mathbf{u}$ is the anti-symmetric version (i.e. $\mathcal{S}\mathbf{u}_A = -\mathbf{u}_A$) because $\mathcal{S}^2 = \mathbf{I}$ the identity. Hence, it is enough to search over purely $\mathcal{S}$-symmetric and $\mathcal{S}$-antisymmetric disturbances when examining the linear stability of $\mathbf{u}_{lam}$.

The last point (c) revolves around the nonlinear term. Defining

$$\mathcal{N}(\mathbf{u}_1, \mathbf{u}_2) := \mathbf{u}_1\cdot\nabla\mathbf{u}_2 + \mathbf{u}_2\cdot\nabla\mathbf{u}_1, \qquad (31)$$

then the nonlinear branch originating from the bifurcating eigenfunction $\mathbf{u}$ will only stay in the same subspace of $\mathcal{S}$ as $\mathbf{u}$ *if*

$$\mathcal{N}(\mathbf{u}_{lam}, \mathbf{u}) \quad \& \quad \mathcal{N}(\mathbf{u}, \mathbf{u})$$

possess the same symmetry under $\mathcal{S}$. Since $\mathbf{u}_{lam}$ is $\mathcal{S}$-symmetric, this means that $\mathbf{u}$ needs to be $\mathcal{S}$-symmetric for the nonlinear solution branch to stay in the $\mathcal{S}$-symmetric subspace. This is the reason why there is a strong (practical) preference to track these types of bifurcation as opposed to the $\mathcal{S}$-antisymmetric bifurcations which immediately break out of the $\mathcal{S}$-antisymmetric subspace (i.e. this subspace is not invariant under the dynamics). The more symmetries that are preserved in the bifurcation the better the efficiency in representing the solution (in terms of number of degrees of freedom to achieve a given spatial resolution) - see figure 3.

1.5 Initializing the Continuation

A good guess is needed to find a solution when using Newton-Raphson especially for a highly nonlinear PDE like the Navier-Stokes equations (see figure 4 for a cautionary tale). This can be produced at the bifurcation point by taking

$$\hat{\mathbf{u}} = \varepsilon\mathbf{u}_1 e^{ikz} + c.c. \quad \& \quad Re = Re_L + \delta \qquad (32)$$

where both ε and δ are small. Weakly nonlinear analysis predicts how they are related as both go to zero but this information is not always available (weakly nonlinear analysis is a tedious mix of integration and solving subproblems for the mean correction
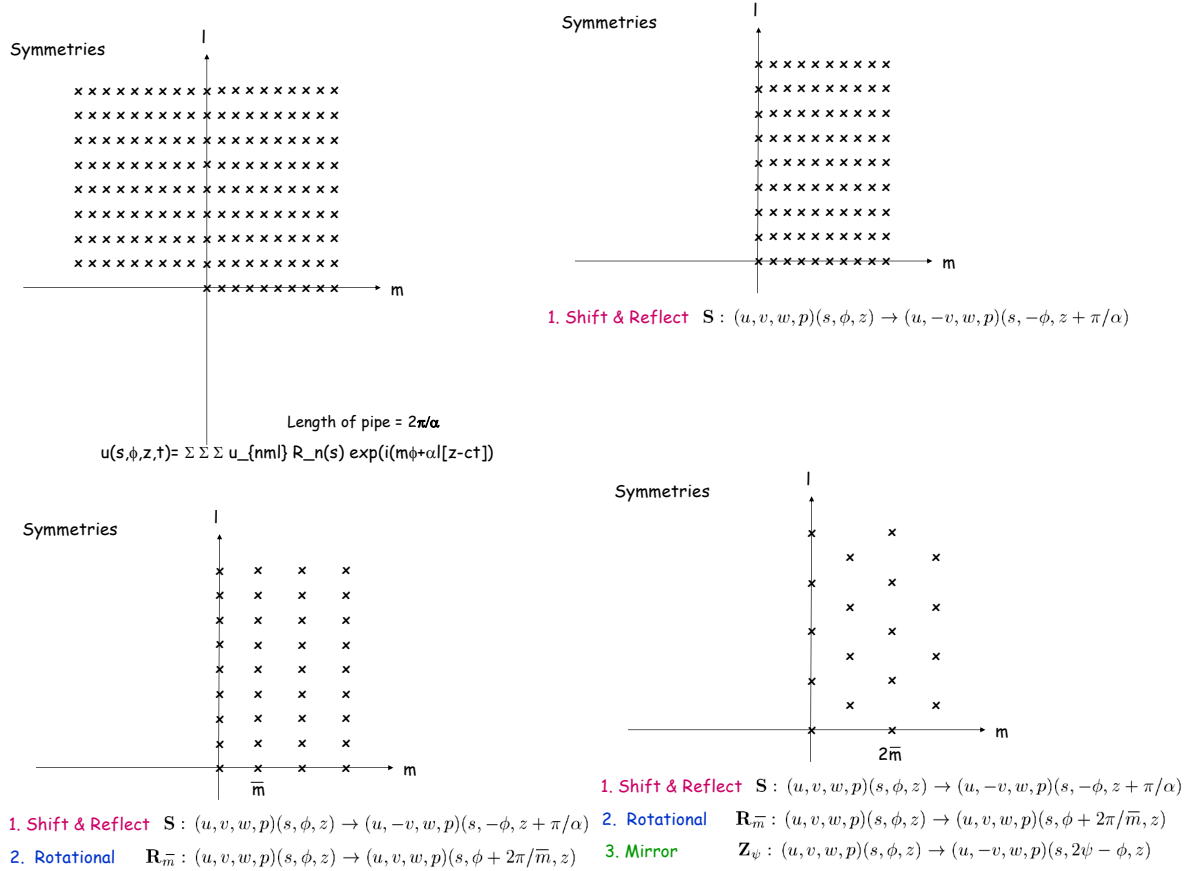
Symmetries

Length of pipe = 2π/α

$u(s,\phi,z,t) = \Sigma\Sigma\Sigma\, u_{\{nml\}}\, R_n(s)\, \exp(i(m\phi+\alpha l[z-ct]))$

Symmetries

1. Shift & Reflect $\mathbf{S}: (u,v,w,p)(s,\phi,z) \to (u,-v,w,p)(s,-\phi,z+\pi/\alpha)$

Symmetries

$\overline{m}$

1. Shift & Reflect $\mathbf{S}: (u,v,w,p)(s,\phi,z) \to (u,-v,w,p)(s,-\phi,z+\pi/\alpha)$
2. Rotational $\mathbf{R}_{\overline{m}}: (u,v,w,p)(s,\phi,z) \to (u,v,w,p)(s,\phi+2\pi/\overline{m},z)$

Symmetries

$2\overline{m}$

1. Shift & Reflect $\mathbf{S}: (u,v,w,p)(s,\phi,z) \to (u,-v,w,p)(s,-\phi,z+\pi/\alpha)$
2. Rotational $\mathbf{R}_{\overline{m}}: (u,v,w,p)(s,\phi,z) \to (u,v,w,p)(s,\phi+2\pi/\overline{m},z)$
3. Mirror $\mathbf{Z}_\psi: (u,v,w,p)(s,\phi,z) \to (u,-v,w,p)(s,2\psi-\phi,z)$

Figure 3: The benefit of imposing symmetries on the numerical representation of a solution. The flow here is pipe flow and the coordinate system is the cylindrical system (s,ϕ,z) where the z-axis is aligned with the pipe axis. The indices m and ℓ refer to Fourier expansions in ϕ and z respectively. In each diagram, the crosses refer to the complex coefficients which need to be stored to represent the solution: the more symmetries which are satisfied by the solution the less coefficients which need to be stored which means branch continuation is more efficient (requires less storage and Newton-Raphson proceeds faster).

$\mathbf{u}_0$ and second harmonic $\mathbf{u}_2$ so usually skipped now). Better to just try a few guesses and see if the algorithm converges to something non-zero (zero corresponds to the unbifurcated solution with no z structure).

Assuming that something has converged at a given Re, continuation is the process of tracing out the curve by using $\mathbf{u}(Re)$ as a guess for $\mathbf{u}(Re + \delta Re)$ where δRe is supposed to be 'small' enough that the guess converges. This simple approach is fine until the branch undergoes a saddle node bifurcation (a.k.a. turns back) where the derivative of how the solution changes with the continuing parameter goes singular. A better approach is to continue using the arc-length as a parameter since this is guaranteed to monotonically increase as the solution branch develops. In fact, an
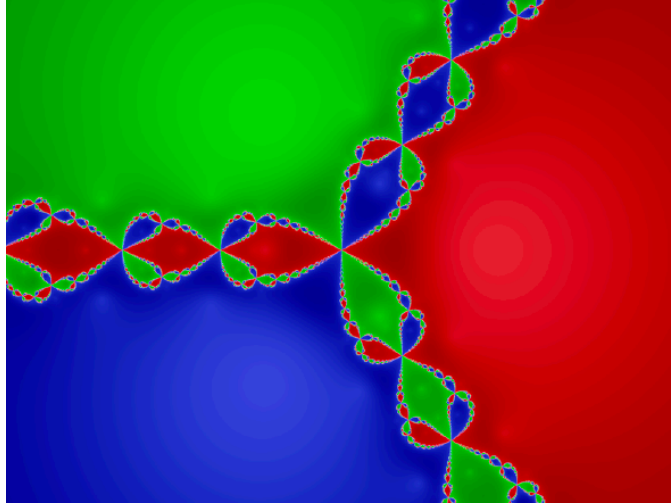
8

Figure 4: The basins of attraction for Newton's method corresponding to the 3 complex roots of $z^3 = 1$ form a well-known fractal ($z = 0$ is the centre of the picture).
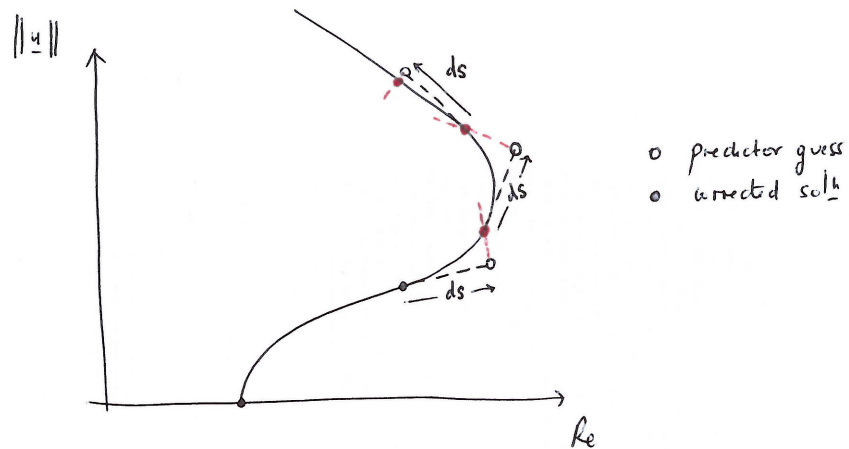

Figure 5: Pseudo-Arclength continuation: u is the dependent variable, Re the parameter being varied and ds is the pseudo arclength (i.e. not the real arclength). The open circles are the predicted solutions and the nearby filled circles are the corrected solutions.

approximation to the arc-length is used in pseudo-arclength continuation which is cheaper and works just as well: see figure 5 and §2.2 in [2] for a discussion.

The result of branch continuing the solutions out of the primary bifurcation from the 1D base state $\mathbf{u}_{\text{lam}} := y\hat{\mathbf{x}}$ to 2D solutions is shown in figure 6 as a blue surface existing at higher Re than that defining the neutral (bifurcation) curve - this indicates
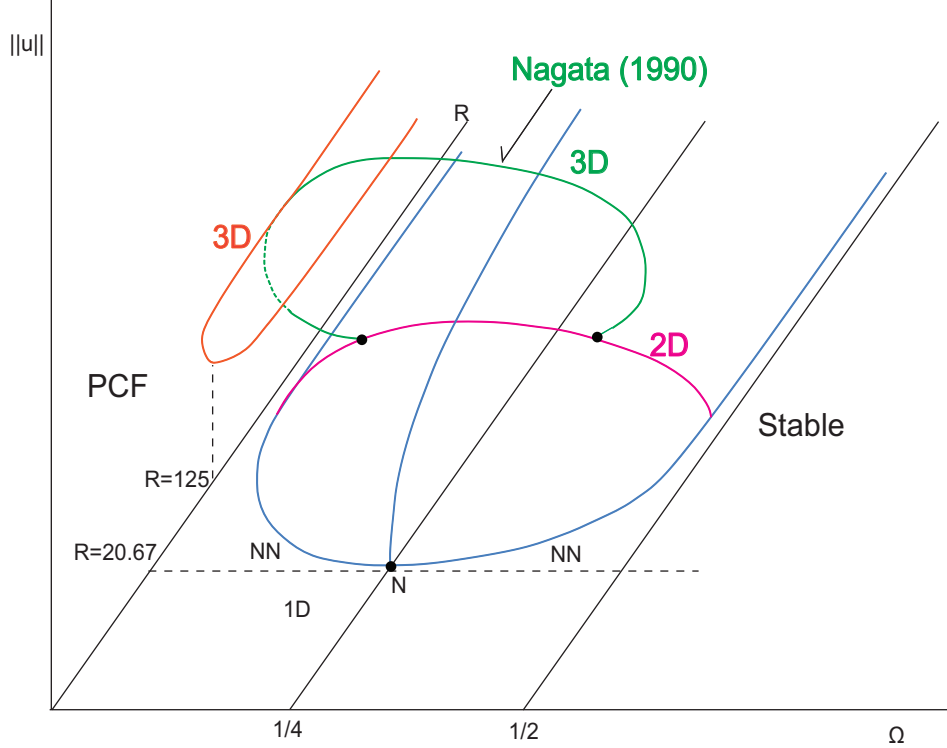
Figure 6: Bifurcation diagram for rotating plane Couette flow.

a supercritical bifurcation (nonlinear solutions exist where the base state is linearly unstable).

1.6   Stability

A green 3D solution curve coming off the 2D surface (along the magenta cross-section) is also shown in figure 6. This is produced by another symmetry-breaking instability where the flow goes from being 2D to 3D. This secondary bifurcation is a linear instability of the 2D solution $\mathbf{u}_{2D}(y,z)$ to an x-dependent eigenfunction of the form

$$\mathbf{u}(y,z)e^{i\alpha(x-ct)} \qquad \text{where } \alpha \in \mathbb{R} \tag{33}$$

and $c \in \mathbb{C}$ is the eigenvalue. A bifurcation occurs where the imaginary part of c vanishes (i.e. $c_i = 0$) for a given α. In fact the solutions shown have $c_r = 0$ so the 3D solutions are steady as well.

This process can be repeated identifying tertiary, quaternary and further bifurcations (Marc Avila will talk more about this) as they arise (typically with increasing Re) and the picture complexifies as 1) solutions become more complicated (spatially and temporally); and 2) multistability may arise (the number of *attractors* increases). This is numerical bifurcation theory as its best: a constructive approach to generating
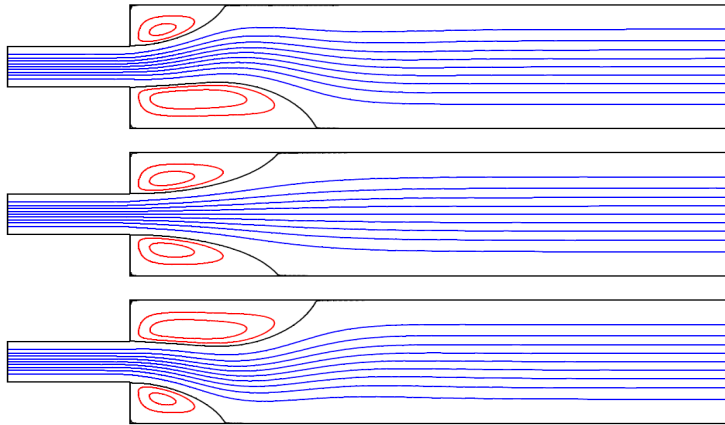
Figure 7: Supercritical bifurcation in a sudden channel expansion. The middle symmetric state is the unstable base state and the top and bottom states are the stable states on the pitchfork arms.
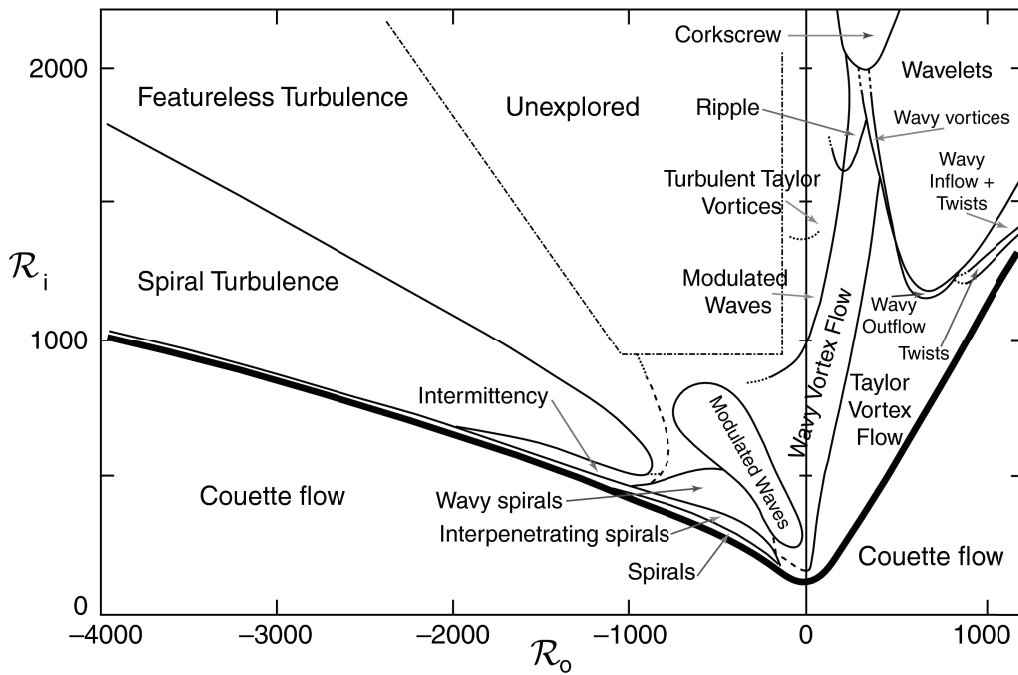

Figure 8: Phase diagram of patterns observed in Taylor-Couette flow as a function of the inner Reynolds number R_i and the outer Reynolds number R_o. The heavy line denotes the boundary between featureless flow below the line and patterned states above the line. (Redrawn from [1], see also [3], figure 7.8).

new solutions and determining attractors as a function of the parameters describing the system; exemplified by sudden expansion flows (see figure 7), Rayleigh-Benard convection and Taylor-Couette studies (see figure 8).
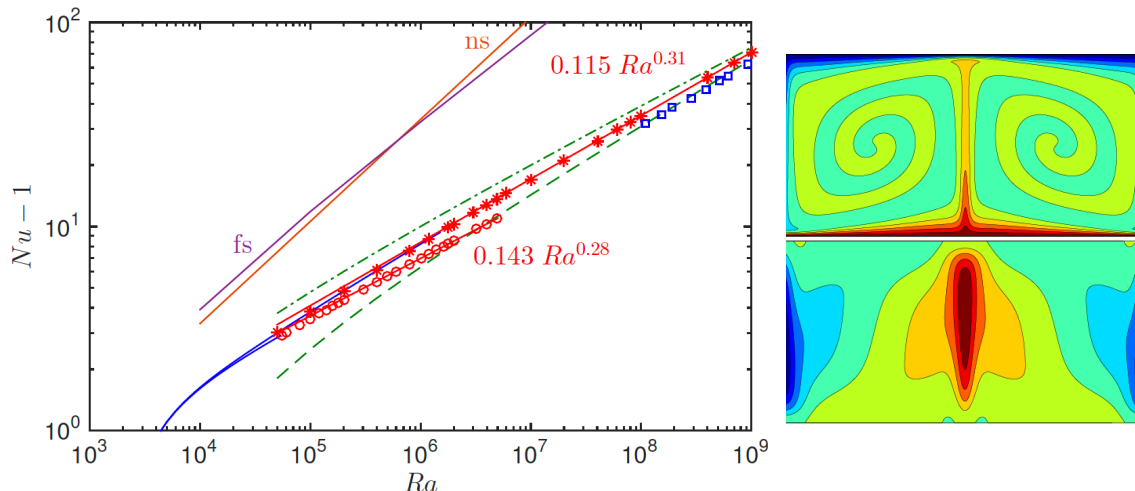

Figure 9: Heat flux in Rayleigh-Benard convection is usually discussed in terms of the Nusselt number Nu which is the ratio of convective heat flux across the layer to the equivalent conductive flux. **Left**: $Nu - 1$ is plotted against Ra (a measure of the boundary heating) for the primary bifurcation branch (red o; $Nu - 1 \sim 0.143 Ra^{0.28}$) and wavelength-optimized branch (red *; $Nu - 1 \sim 0.115 Ra^{0.31}$). Upper dash-dot green curve is 3D turbulent data $Nu - 1 \sim 0.23 Ra^{0.28}$ and lower dash green curve is the 3D turbulent data $Nu \sim 0.088 Ra^{0.32}$. The line 'fs' is the free-slip upper bound $Nu \lesssim 0.106 Ra^{5/12}$ and the 'ns' line is the no-slip upper bound $Nu \lesssim 0.0335 Ra^{1/2}$ (this is figure 2 from [13]). **Right**: temperature field (upper) and velocity (lower) for optimal 2D solution.

Unstable states can also be physically relevant. Figure 9 plots the heat flux associated with the primary branch of convective rolls which bifurcate off the conductive (fluid at rest) state [13]. Even though this solution is unstable, the heat flux associated with it appears to closely resemble that measured on average for turbulent convection. A plausible interpretation is that the flow is repeatedly attracted back to the roll solution before being repelled so that on average, the turbulent flow approximates it. Efforts are underway to substantiate this. More generally, the fact that unstable solutions can have an important influence in fluid flows is a relatively recent realisation (last 2 decades?). The next topic develops this further.

1.7   Saddle Node Bifurcations

Some canonical problems have a base solution which is always linearly stable (i.e. even as $Re \to \infty$): for example, plane Couette flow ([8] has a proof) and pipe flow (no formal proof yet but see [5] for numerical verification up to $Re = 10^7$). In this
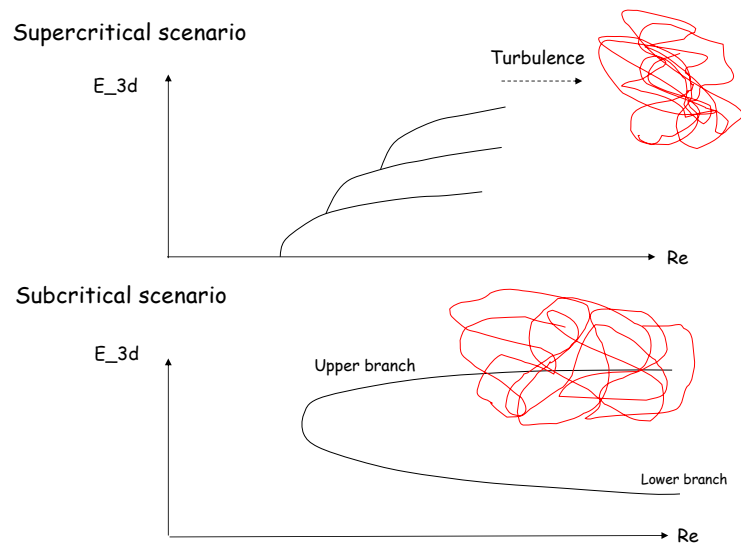
Figure 10: Supercritical (top) and Subcritical (bottom) scenarios in fluid flows. Examples of the former are Rayleigh-Benard convection and Taylor-Couette flow (when the inner cylinder rotates faster than the outer), whereas shear flows such as plane Couette flow and pipe flow typify the latter (formally, plane Poiseuille flow is a mixture - it has a linear instability [7] but this is typically not important in the transition to turbulence seen in experiments)

case, it is not clear how to progressively construct new solutions or even if they exist (and are dynamically significant). The generic way phase space can complexify is through saddle node bifurcations in which pairs of solutions spontaneously form: see figure 10. Finding these bifurcations is very hard without some clue.

One very general approach is Homotopy in which solutions are smoothly continued from one problem where they are known to (hopefully) another where they are not. Typically, the problem of interest is embedded in a bigger problem which does have a bifurcation to follow: see figure 11. Using this approach, Nagata [6] famously traced steady 3D solutions in rotating plane Couette flow around in (Re, Ω) parameter space, until they crossed the $\Omega = 0$ plane for $Re \geq 125$ (later more accurately computed to be 127.7 [12]): see figure 6. These non-rotating steady 3D solutions (shown in red) were the first discovery of exact solutions to plane Couette flow beyond the simple constant shear state. The approach doesn't always works, however: see figure 12.

It helps to have some understanding of what the underlying structure of the solutions is. In unidirectional shear flows, we now know that solutions borne in saddle node bifurcations generically have a tripartite structure consisting of streamwise rolls, streaks and a streamwise-dependent wave [4, 11]: see figure 13. Knowing this helps to design a homotopy which was what Waleffe [11] famously did following the suggestive
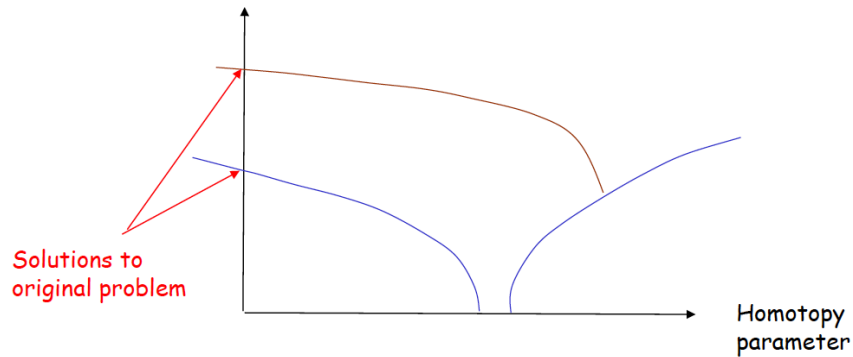
13

Figure 11: Homotopy is the technique for linking solutions in one problem to another. Typically, the problem of interest is embedded in a bigger problem with an extra homotopy parameter where there is a nearby bifurcation. Ideally, the bifurcated (primary) branch of solutions immediately bends towards and crosses the limiting situation of the original problem of interest (homotopy parameter vanishes). If not, it might still be possible to achieve this but after finding and tracking further (secondary, tertiary,...) bifurcations.

calculations of [4]. The key idea was to add an artificial forcing into the Navier-Stokes equations (the embedding problem needn't correspond to a physical system although this is obviously preferable) to generate small-amplitude streamwise rolls (see figure 14). These then create much larger amplitude streaks - deviations of the streamwise velocity field from the base flow - via advection of the base flow. If the added force is large enough, these streaks are inflectionally unstable to streamwise-dependent waves. Then if these waves are of the right structure to feed energy into the streamwise rolls, the force can be reduced as the amplitude of the branch grows and ideally, the axis of zero forcing is reached. At this point, a finite-amplitude solution to the unforced Navier-Stokes equations is identified. Typically, the solution branch bends back to recross the axis delivering two solutions representing he upper and lower branch solutions of a saddle node bifurcation as in figure 15 but more complicated things can happen yielding more solutions than expected: see figure 16.
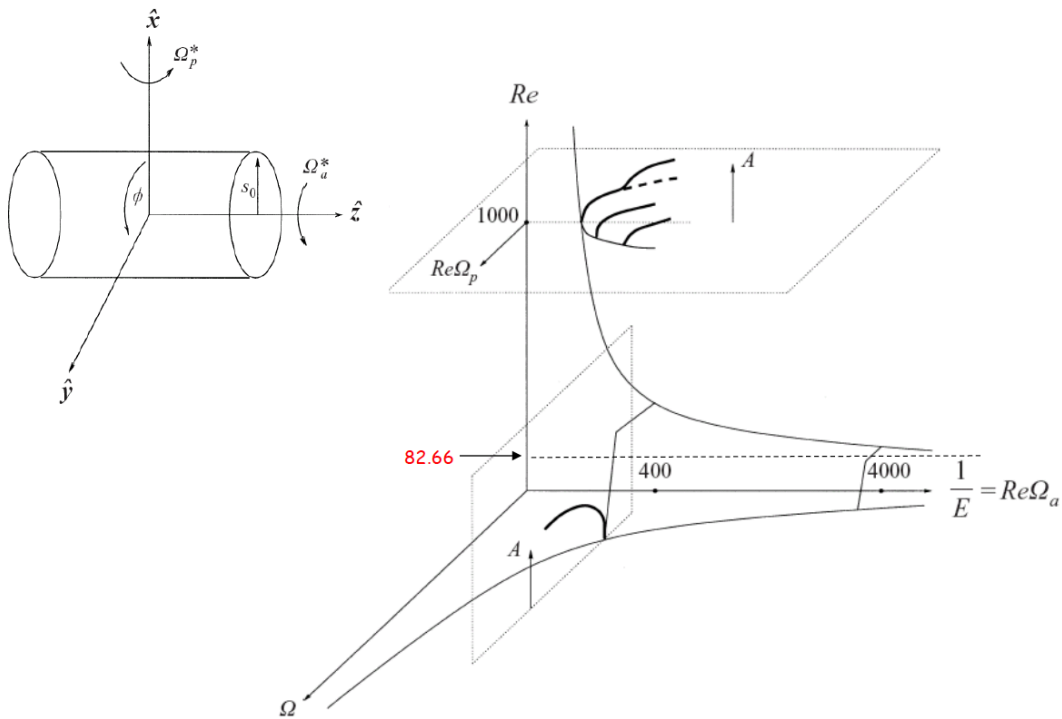
14

Figure 12: Failed homotopy in rotating pipe flow: solution branches bend away from the non-rotating limit (the axis when $\Omega = \Omega_a = 0$).
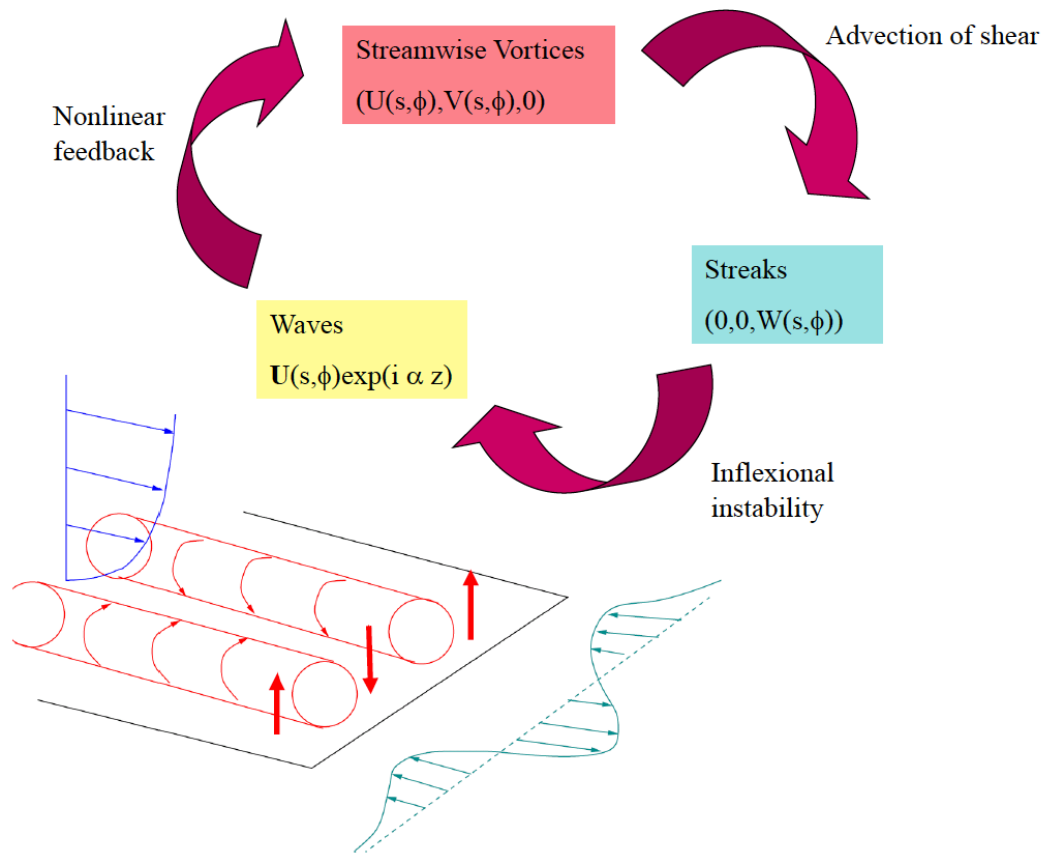
Figure 13: The Self-Sustaining Process (SSP) [11]. Streamwise rolls advect the base shear to produce streaks which, when they have largest enough amplitude, are inviscidly unstable to (streamwise-dependent) waves. Some of the these waves can constructively interfere to energise the streamwise rolls to close the dynamical cycle of structures.

Continuation strategy

$$\partial_t U + P_s - \frac{1}{Re}\widehat{\boldsymbol{s}}.\nabla^2 \mathbf{U} + \widehat{\boldsymbol{s}}.(\mathbf{U}.\boldsymbol{\nabla}\mathbf{U}) = f_s(s,\phi) - \widehat{\boldsymbol{s}}.(\overline{\widehat{\boldsymbol{u}}.\boldsymbol{\nabla}\widehat{\boldsymbol{u}}}^z),$$

$$\partial_t V + \frac{1}{s}P_\phi - \frac{1}{Re}\widehat{\boldsymbol{\phi}}.\nabla^2 \mathbf{U} + \widehat{\boldsymbol{\phi}}.(\mathbf{U}.\boldsymbol{\nabla}\mathbf{U}) = f_\phi(s,\phi) - \widehat{\boldsymbol{\phi}}.(\overline{\widehat{\boldsymbol{u}}.\boldsymbol{\nabla}\widehat{\boldsymbol{u}}}^z)$$
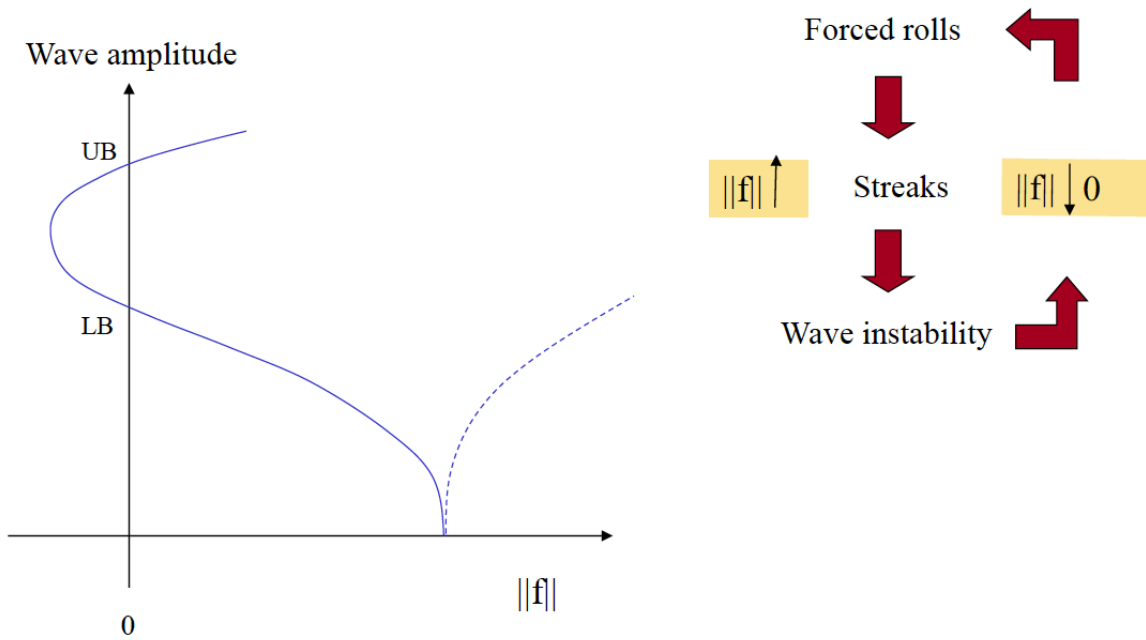

Figure 14: Homotopy procedure suggested by SSP. $(U,V) = (U(s,\phi), V(s,\phi))$ are the streamwise rolls (independent of the streamwise coordinate z). f is the artificial forcing which initially drives the rolls which then generate streaks. Once these streaks reach a certain amplitude, there is a bifurcation, which, if the instability is of the right type, can be traced back to the $f = 0$ axis indicating an exact solution to the Navier-Stokes equations in pipe flow [14].
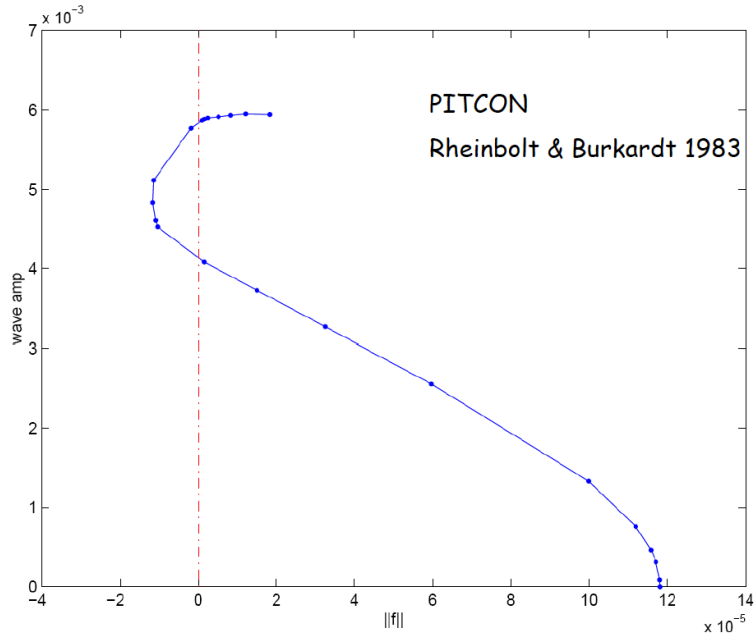
Figure 15: Successful homotopy: the artificial forcing f has been reduced to 0 thereby identifying 2 solutions of the unforced Navier Stokes equations with pipe flow boundary conditions and pressure gradient forcing [14].
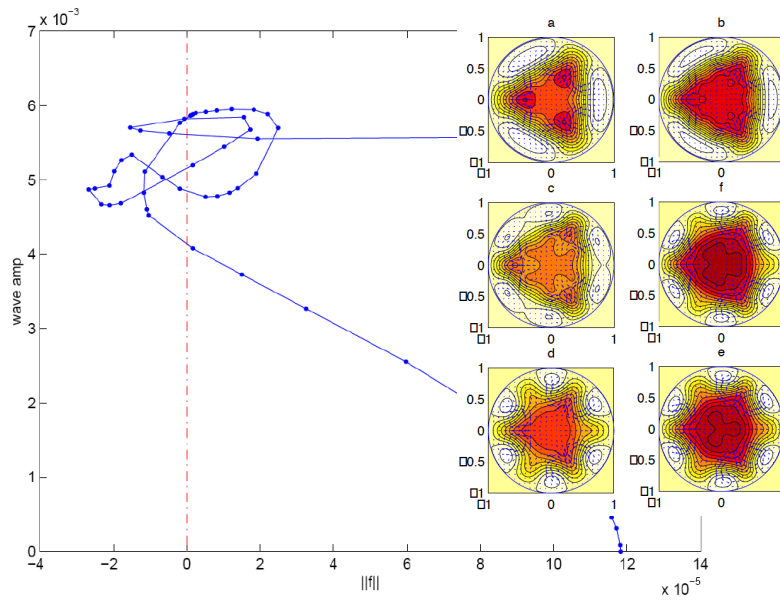

Figure 16: Multiple crossings mean multiple new solutions. The inset cross-sections detail the six solutions corresponding to the crossings (colours indicate streamwise anomaly relative to the laminar state for constant pressure gradient flow [14].

1.8 Summary

Here's a quick recap of the topics covered in these two lectures.

(*i*) Weakly nonlinear analysis considers the first influence of nonlinearity to build a solution branch out of a bifurcation based on the neutral eigenfunction.

(*ii*) Branch continuation extends weakly nonlinear analysis to finite amplitude.

(*iii*) Symmetry considerations are fundamental to branch continuation and identifying bifurcations.

(*iv*) Flows where the base flow becomes linearly unstable offer a natural beechhead to find new attractors.

(*v*) For linearly-stable base flows, saddle-node bifurcations are generic and homotopy is the main tool for finding them.

References

[1] C. D. ANDEREK, S. S. LIU, AND H. L. SWINNEY, *Flow regimes in a circular Couette system with independently rotating cylinders*, J. Fluid Mech., 164 (1986), pp. 155–183.

[2] H. A. DIJKSTRA, F. W. WUBS, A. K. CLIFFE, E. DOEDEL, I. F. DRAGOMIRESCU, B. ECKHARDT, A. Y. GELFGAT, A. L. HAZEL, V. LUCARINI, A. G. SALINGER, E. T. PHIPPS, J. SANCHEZ-UMBRIA, H. SCHUTTELAARS, L. S. TUCKERMANN, AND U. THIELE, *Numerical bifurcation methods and their application to fluid dynamics: Analysis beyond simulation*, Commun. Comput. Phys., 15 (2014), pp. 1–45.

[3] P. G. DRAZIN, *Introduction to Hydrodynamic Stability*, Cambridge University Press, second ed., 2002.

[4] J. M. HAMILTON, J. KIM, AND F. WALEFFE, *Regeneration mechanisms of near-wall turbulence structures*, J. Fluid Mech., 287 (1995), pp. 317–348.

[5] A. MESEGUER AND L. N. TREFETHEN, *Linarized pipe flow to Reynolds number 10(7)*, Journal of Computational Physics, 186 (2003), pp. 178–197.

[6] M. NAGATA, *Three-dimensional finite-amplitude solutions in plane Couette flow: bifurcation from infinity*, J. Fluid Mech., 217 (1990), pp. 519–527.

[7] S. A. ORSZAG, *Accurate solution of the Orr-Sommerfeld stability equation*, J . Fluid Mech., 50 (1971), pp. 659–703.

[8] V. A. ROMANOV, *Stability of plane Couette flow*, Funckional Anal. i Prolozen, 7 (1973).

[9] L. N. TREFETHEN, *Spectral Methods in Matlab*, (2000).

[10] L. VAN VEEN, *A brief history of simple invariant solutions in turbulence*, Computational Modelling of Bifurcations and Instabilities in Fluid Dynamics (ed. E. Gelfgat), Springer series on Computational Methods in Applied Sciences, 50 (2018).

[11] F. WALEFFE, *On a self-sustaining process in shear flows*, Phys. Fluids, 9 (1997), pp. 883–900.

[12] F. WALEFFE, *Homotopy of exact coherent structures in plane shear flows*, Phys. Fluids, 15 (2003), pp. 1–18.

[13] F. WALEFFE, A. BOONKASAME, AND L. M. SMITH, *Heat transport by coherent Rayleigh-Benard convection*, Phys. Fluids, 27 (2015), p. 051702.

[14] H. WEDIN AND R. R. KERSWELL, *Exact coherent structures in pipe flow: travelling wave solutions*, J. Fluid Mech., 508 (2004), pp. 333–371.